

N87-26544

RECONSTRUCTION OF CODED APERTURE IMAGES

Michael J. Bielefeld

Astronomy Programs, Computer Sciences Corporation
Space Telescope Science Institute
3700 San Martin Dr. Baltimore, MD 21218

Lo I Yin

Code 682, Solar Physics Branch
Laboratory for Astronomy and Solar Physics
NASA Goddard Space Flight Center, Greenbelt, MD 20771

ABSTRACT

Balanced correlation method and the Maximum Entropy Method (MEM) were implemented to reconstruct a laboratory x-ray source as imaged by a Uniformly Redundant Array (URA) system. Although the MEM method has important physical advantages over the balanced correlation method, it is computationally time consuming because of the iterative nature of its solution. MPP, with its parallel array structure is ideally suited for such computations. These preliminary results indicate that it is possible to use the MEM method in future coded-aperture experiments with the help of the MPP.

must resort to the use of collimators or pinholes made from high density materials. In this paper, we will focus on the use of pinholes.

Because a single pinhole is extremely inefficient, there is a strong interest in the use of multiple pinholes to image x-ray objects [1-12]. However, in most cases, the images on the detector formed by the many pinholes strongly overlap each other resulting in a detected image that is not recognizable. A decoding process must then be applied to the detected image in order to recover or reconstruct the image of the original object. Such multiple-pinhole masks are usually referred to as coded apertures.

INTRODUCTION

In the energy range of hard x-rays, i.e., 30 keV to 100 keV, there is no focusing optics. Consequently, in order to image the many interesting objects which emit radiations in this energy range such as galaxies, the sun, nuclear reactor components, and human organs tagged with radioisotopes, one

In principle, the large collection efficiency (close to 50%) of coded apertures offer the possibility of a greatly enhanced signal-to-noise ratio while maintaining the high spatial resolution of a single pinhole. Furthermore, for terrestrial applications, coded apertures can provide tomographic information of the x-ray object. In practice, however, there are

several difficulties associated with the use of coded apertures, especially in the imaging of extended or large x-ray objects. Because of the strongly overlapping images on the detector, the signal in one location of the reconstructed image may contain contributions from all other portions of the object. This type of signal cross-talk is object-dependent and can be present in addition to statistical noise. Such signal-cross talk can cause severe contrast degradation in the reconstructed image of extended objects. There has been many studies in recent years on the performance properties of various kinds of coded apertures. One of the most promising type of coded apertures is the Uniformly Redundant Array (URA) [10,11]. A URA is a special kind of multiple-pinhole mask in which the number of times a particular separation occurs between any pair of pinholes is the same for all separations. The separations are therefore uniformly redundant. URA has some very desirable properties; one of which is that with proper decoding the signal cross-talk mentioned above can be eliminated completely. However, noise cross-talk still exists. That is, the statistical noise from one part of the object can still contribute to the signal of another part in the reconstructed image.

A few years ago, we proposed another simple alternative: the Non-Overlapping Redundant Array (NORA) [12]. It consists of a regular array of pinholes (e.g., a hexagonal array) where the separation between pinholes as well as the separation between

the NORA mask and the detector can be carefully chosen such that the images on the detector formed by the individual pinholes do not overlap. We have shown that in NORA, there is neither signal cross-talk nor noise cross-talk in the reconstructed image and the only inherent noise in the system is that due to counting statistics. The signal-to-noise ratio of NORA, assuming Poisson statistics, is always square-root of N times that of a single-pinhole camera, where N is the total number of pinholes. This is true even for extended objects and is the ideal limit achievable by a multiple-pinhole system. Another important feature of NORA is that it is possible to reconstruct the extended x-ray object in 3-D by simple optical correlation. We have already demonstrated in the laboratory that the optically reconstructed image can be viewed in true 3-D with both horizontal and vertical parallax. In addition, NORA should also provide quantitative tomographic information through digital reconstruction. It is this latter goal that prompted us to seek out the capabilities of the Massively Parallel Processor (MPP).

DIGITAL DECODING

General

Although it is possible to reconstruct an image by analog method when NORA is used as the coded aperture, digital reconstruction is mandatory when the coded aperture, such as URA, produces overlapping images on the detector. Furthermore, to obtain quantitative tomographic

information, digital computation is always necessary.

In digital decoding, the large number of pinholes, pixels and mathematical operations demand large amounts of computing time even with available fast algorithms. At present, because we are still investigating various coding and decoding methods which involve many repeated trials and iterative calculations, long computation times and turn around delays can be both costly and frustrating. The MPP, with its parallel array structure is ideally suited for this type of computations. In fact, as we will show below, the MPP makes our investigations feasible, while the conventional mainframe computer, in normal use, has proven to be inadequate.

Decoding Methods for URA

Balanced Correlation Method - Because of the uniformly redundant and the cyclic nature of the URA, its point spread function is a delta function with constant and flat sidelobes. That is, if the object is a point source and is detected by an ideal URA system, the decoded image by means of an autocorrelation operation will be also a point source (delta function), but with a constant and uniform background. This flat dc background can be eliminated by using the balanced correlation method. In this method, although the decoding array has the same pattern as the coding URA array with 1's representing the holes, the non-holes are represented by -1's rather than 0's [10]. However, in contrast to well-separated point sources, noise due to

statistical fluctuations in the background which is not aperture related can still contribute to the reconstructed signal as the object gets large, even with balanced correlation decoding. This kind of noise cross-talk may give rise to artifacts in the low-contrast background region of the reconstructed image.

Maximum Entropy Method (MEM) - Recently many investigators have become interested in applying the maximum entropy method (MEM) to the field of image restoration including the reconstruction of coded-aperture images [13-18]. MEM is an iterative method which maximizes the configurational entropy while using prior knowledge such as chi-squared (X^2) statistic and total detected intensity as constraints. Through iteration, the solution with the maximum configurational entropy, i.e., with the least configurational information, is selected from a set of solutions all of which satisfy the chi-squared fit of the actual data. This solution is considered as the most likely estimate of the original object that is consistent with the available data.

Following Willingale [15], the solution has the form:

$$\hat{f}_i^m = z_i e^{-(\mu + 1)}, \quad (1)$$

$$e^{-2\lambda \left[\sum_K B_{Ki} (\hat{d}_K - d_K) / \sigma_K^2 \right]}$$

where (\hat{f}_i^m) is the estimated intensity of the i th pixel of the object as seen by the instrument which maximizes the

configurational entropy
 $[- \sum \hat{f}_i \ln \hat{f}_i + \sum \hat{f}_i \ln z_i]$; (z_i)
 is the instrument efficiency,
 i.e. (f_i / z_i) is the true
 intensity of the i th pixel of the
 object; (B_{ki}) is the transpose of
 the blurring matrix of the coded
 aperture; (d_k) is the actual data
 on the detector; (\hat{d}_k) is an
 estimated data, without noise,
 which would be produced on the
 detector if the object were
 correctly represented by (\hat{f}_i);
 (σ_k^2) is the variance of the data
 (d_k); (λ) and (μ) are Lagrange
 multipliers. The function Q
 which is being maximized to
 produce the solution as
 represented by Equation (1) is:

$$Q = - \sum_i \hat{f}_i \ln \hat{f}_i + \sum_i \hat{f}_i \ln z_i$$

$$(2)$$

$$- \lambda \sum_i (\hat{d}_i - d_i)^2 / \sigma_i^2 + \mu \sum_i \hat{f}_i$$

The first two terms of (2)
 comprise the configurational
 entropy; the third term with the
 Lagrange multiplier (λ) is the
 (X^2), and the fourth term with
 Lagrange multiplier (μ) is the
 total intensity of the object.
 For large number of data points
 N , (X^2) $\cong N$. To conserve total
 counts, ($\sum \hat{f}_i = \sum \hat{d}_i$).
 Noise in the data is accounted
 for by the variance (σ_k^2).

There are several important
 advantages in using (1) as the
 decoding solution. Because (1)
 is in the exponential form, this
 solution is never negative. The
 first exponential is a constant
 scaling factor which gives the
 reconstruction a uniformly
 distributed intensity without

features. When the noise in the
 data is very high, this
 featureless solution ($\lambda=0$) will
 be consistent with the data, (\hat{f}_i^m)
 will be simply proportional to
 (z_i) by maximum configurational
 entropy. When the signal in the
 data is high, the featureless
 background as given by the first
 exponential will be modulated by
 the features provided by the
 second exponential. The
 summation in the second
 exponential represents a
 cross-correlation between the
 blurring function of the coded
 aperture and the difference
 between the estimated data and
 the actual data weighted by its
 statistical variance. Since this
 reconstruction occurs in the
 exponential, iterative algorithms
 are needed for its solution.

The relative weighting of entropy
 and (X^2) is controlled by (λ).
 As mentioned above, when (λ) = 0,
 (X^2) has no weighting, and the
 solution is a uniform
 distribution as given by maximum
 entropy. When (λ) is increased,
 the process reduces (X^2). A
 final (λ) will be selected when
 (X^2) becomes close to N , the
 expected value. To help
 convergence, we also adopted the
 search algorithm of Willingale
 [15] by taking weighted averages
 of successive iterations.

EXPERIMENTAL DATA

As an initial test toward digital
 decoding using the MPP we have
 chosen some data which we had
 obtained previously with a URA
 coded aperture. The experimental
 arrangement is sketched in Figure
 1. The URA mask consisted of a
 two-cycle mosaic of a basic 15 x
 17 m-sequence array. The

pseudo-random m-sequence pattern was generated according to the procedure given by MacWilliams and Sloane [19]. The pattern was drilled into a 0.5-mm thick Pb sheet by a computer-driven lathe. The holes were 0.3 mm in diameter; the center-to-center separation of adjacent holes was 0.6 mm. Thus, the transparency of this mask was about 10%. For the imaging detector, we used a Lixiscope [20] with a digitizing anode. Briefly, for the present data, the Lixiscope consisted of a thin layer of $\text{YSiO}_3(\text{Ge})$ powder serving as an x-ray to visible light converter which was deposited on the entrance faceplate of a 1:1 image intensifier containing a triple microchannel-plate (MCP) electron multiplier [21]. The output electron signals from the triple MCP are detected by a resistive anode which can provide both the position and the amplitude of an electron pulse. For the simplest case of the present experiment a single small I-125 x-ray source (28 keV) was used as the x-ray emitting object. The distance between the source, the mask and the Lixiscope were chosen such that the sensitive area of the detector recorded at least one complete basic array of the magnified shadow of the two-cycle URA mask. The experimental image of the source, which was positioned at 31 cm from the detector, is shown in the upper left corner of Figure 2. The display exaggerates the contrast in the data for this array of 256×256 pixels. The average counts per pixel is about 2. Because the emitting object is a point source, the basic URA pattern is clearly visible within the circular active area of the detector. The digitized version

of this image (Fig. 2) is used as the data to be decoded by both the balanced correlation method and the MEM.

DECODING OF URA IMAGE

The basic implementations of the balanced correlation method and the MEM are relatively straightforward. However, an important distinction should be mentioned between this type of x-ray image processing and that of the more common visible/IR image processing. In our case, one is dealing with extremely low count rates. Because of this, the statistical uncertainty of individual pixels has to be followed through the decoding process at the basic level of computation. The formalism for the MEM in Equation (1) takes full account of this requirement.

The specification of spatial resolution for the experimental system displayed in Figure 1 includes not only resolution in the x-y plane but also in the z direction. Hence, the digital decoding of 3-D objects requires much finer sampling than the basic pinhole array. This requirement for high sampling rates along with the iterative nature of the MEM are the main factors which directed us toward using the MPP.

The decoding process requires at a minimum sampling rate of 17×15 pixels per cycle of the URA. Because the detected image (Fig. 2, top left) is an array of 256×256 pixels, this image is collapsed to the minimum array of 17×15 through summing as shown in Figure 2, top right. This

coded image is almost featureless. The bottom images of Figure 2 show the results of digital decoding by the MEM (left) and the balanced correlation method (right). Both methods clearly reconstructs the point source to the same degree. However, these images illustrate several advantages of the MEM. First, the MEM does not permit the physically impossible negative counts seen in the background region of the image reconstructed by the balanced correlation method (bottom right). Secondly, the MEM produces a much smoother background (bottom left). This smoothness helps to minimize the erroneous interpretation of artifacts arising from noise cross-talk.

As mentioned earlier, the iterative process should be terminated when (X^2) become close to N , the number of data points. Letting (X^2) to reduce further will only add artifacts to the already smooth background. (λ) controls the relationship between the entropy portion and the data portion in Equation (1).

For extended objects with unknown shapes, the smoothing capability of the MEM becomes even more important than for points sources. In our opinion, this capability of suppressing background artifacts amply justifies the computational expense of the MEM. Timing experiments on the MPP indicate that MEM decoding of our x-ray URA data is indeed feasible. In general, the MEM requires approximately ten times more computational power than the balanced correlation method because of the iterations. The

CPU requirements for the basic filtering kernel calculation increases as the factor N for the MPP, but as the square of N for a typical mainframe computer, where N is the total number of pixels in a decoded data array. For a future experiment which requires the reconstruction of five tomographic planes at ten iterations per plane with three values of (λ) , our estimate is that decoding would take 1.5 minutes of MPP/CPU time for the minimum sampling rate of 17×15 . At a very high rate of 170×150 pixels per URA cycle, it would take about 2 hours. A compromising sampling rate of 51×45 would take about 12 minutes. Even for this compromised level of decoding, we estimate that the equivalent processing on a large

un-vectorized mainframe would take in excess of 24 hours of CPU time.

CONCLUSIONS

The results of our work to date have been encouraging. The continuation of this research would be greatly enhanced with the computational power of the MPP. We need trial-and-error experience to find the optimum decoding algorithms as experimental configurations are refined, and to determine the practical tomographic depth resolution for 3-D x-ray objects. Our near future plans include the decoding of x-ray data obtained with NORA aperture using the MPP.

ACKNOWLEDGMENT

We acknowledge the continued support of our investigations from within NASA, especially the

MPP Working Group. It is a pleasure to thank Judy Devaney of SAR Corp. and of the MPP supporting staff for her invaluable insights and assistance. We are also indebted to D. Vitagliano and V. Krueger for their technical assistance with the manuscript.

REFERENCES

1. J.G. Ables, Proc. Astron. Soc. Aust. 1, No. 4. 172 (1968).
2. R.H. Dicke, Astrophys. J. 153, L101, (1968).
3. H.H. Barrett and F.A. Horrigan, Appl. Opt. 12, 2686, (1973).
4. T.M. Palmieri, Astrophys. Space Sci. 26, 431, (1974); 28, 277 (1974).
5. C. Brown, J. Appl. Phys. 45, 1806, (1974).
6. B. MacDonald, L.T. Chang, V. Perez-Mendez, and L. Shiraishi, IEEE Trans. Nucl. Sci. NS-21, 672, (1974).
7. R.G. Simpson, H.H. Barrett, J.A. Suback, and H.D. Fisher, Opt. Eng. 14, 490, (1975).
8. F. Gunsen and B. Polychronopoulos, Mon. Not. R. Astron. Soc. 177, 485, (1976).
9. L.T. Chang, B. MacDonald, and V. Perez-Mendez, Proc. Soc. Photo-Opt. Instrum. Eng. (SPIE) 89, 9 (1976).
10. E.E. Fenimore and T.M. Cannon, Appl. Opt. 17, 337, (1978); 18, 1052, (1979).
11. E.E. Fenimore, Appl. Opt. 17, 3562, (1978).
12. L. Yin, J. Trombka, S. Seltzer, and M. Bielefeld, Appl. Opt. 22, 2155 (1983).
13. S.F. Gull and G.J. Daniell, Nature 272, 686, (1978).
14. M. Sims, M.J.L. Turner, and R. Willingale, Space Sci. Instrum. 5, 109, (1980).
15. R. Willingale, Mon. Not. R. Astr. Soc. 194, 359, (1981).
16. S.F. Burch, S.F. Gull, and J. Skilling, Computer Vision, Graphics, and Image Processing 23, 113, (1983).
17. R. Willingale, M.R. Sims, and M.J.L. Turner, Nucl. Instrum. & Methods in Phys. Res. 221, 60, (1984).
18. S.F. Gull and T.J. Newton, Appl. Opt. 25, 156, (1986).
19. F.J. MacWilliams and N.J.A. Sloane, Proc. IEEE 64, 1715, (1976).
20. L. Yin, J. Trombka, and S. Seltzer, Nucl. Instrum. & Methods 158, 175, (1979).
21. L. Yin, J. Trombka, R. Schmadebeck, S. Seltzer, and M. Bielefeld, SPIE 268, 97, (1981).

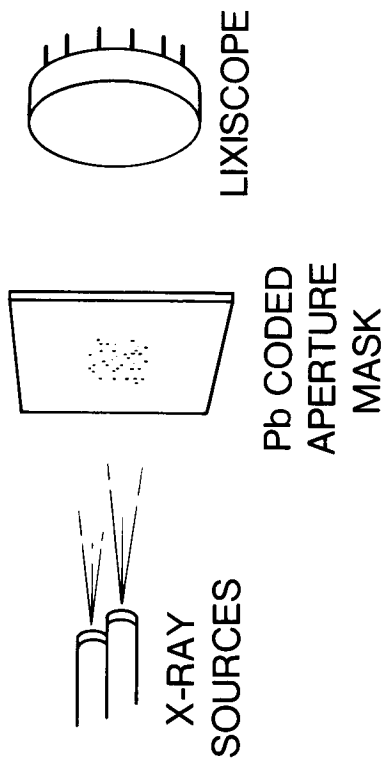
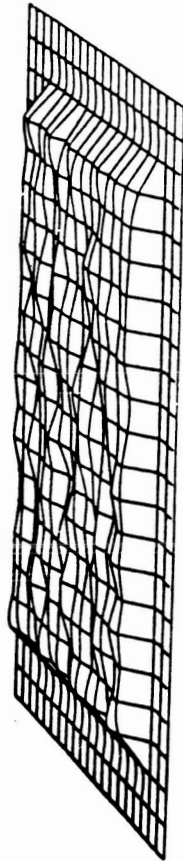


Figure 1. Sketch of experimental setup.

Total Detector Array



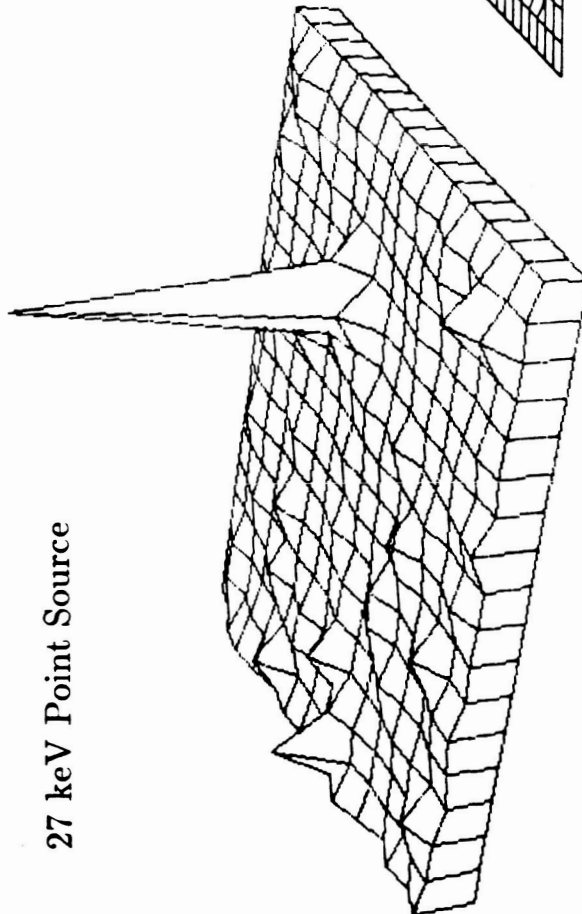
Subsection of Detector Array
(for an Object at 31 cm)



ORIGINAL PAGE IS
OF POOR QUALITY

CODED

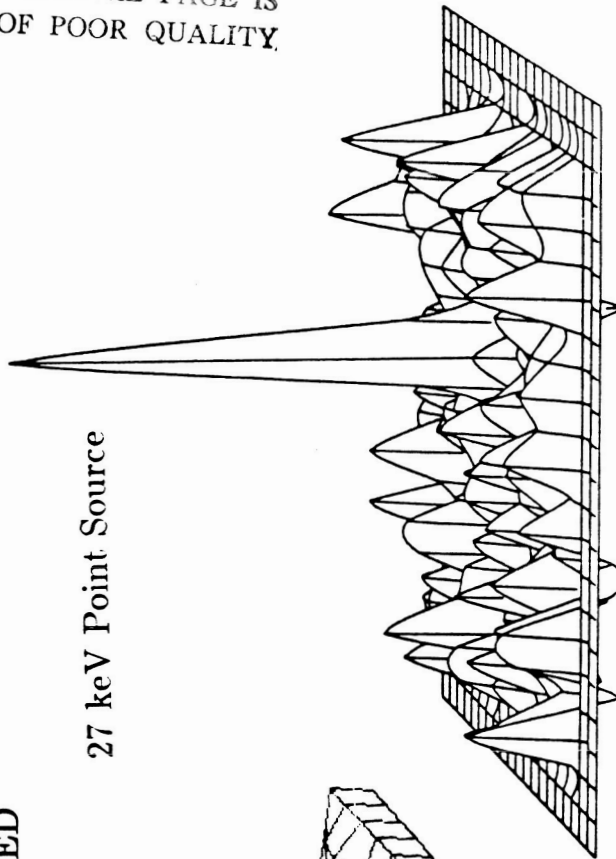
27 keV Point Source



DECODED

(Maximum Entropy Method)

27 keV Point Source



DECODED

(Autocorrelation Method)

Plane at 31 cm

Figure 2. Coded and decoded images of a point source using URA. Top left: original data. Top right: digitized data. Bottom: decoded images by two different methods.